

NRSurNN3dq4: A Deep Learning Powered Numerical Relativity Surrogate for Binary Black Hole Waveforms

Oswaldo Gramaxo Freitas,^{1,2,*} Anastasios Theodoropoulos,² Nino Villanueva,^{3,2} Tiago Fernandes,^{1,2} Solange Nunes,¹ José A. Font,^{2,4} Antonio Onofre,¹ Alejandro Torres-Forné,^{2,4} and José D. Martín-Guerrero^{3,5}

¹*Centro de Física das Universidades do Minho e do Porto (CF-UM-UP),
Universidade do Minho, 4710-057 Braga, Portugal*

²*Departamento de Astronomía y Astrofísica, Universitat de València,
Dr. Moliner 50, 46100, Burjassot (València), Spain*

³*IDAL, Electronic Engineering Department, ETSE-UV, University of Valencia,
Avda. Universitat s/n, 46100 Burjassot, Valencia, Spain*

⁴*Observatori Astronòmic, Universitat de València,
Catedrático José Beltrán 2, 46980, Paterna (València), Spain*

⁵*Valencian Graduate School and Research Network of Artificial Intelligence (ValgrAI), Spain*
(Dated: December 11, 2024)

Gravitational wave approximants are widely used tools in gravitational-wave astronomy. They allow for dense coverage of the parameter space of binary black hole (BBH) mergers for purposes of parameter inference, or, more generally, match filtering tasks, while avoiding the computationally expensive full evolution of numerical relativity simulations. However, this comes at a slight cost in terms of accuracy when compared to numerical relativity waveforms, depending on the approach. One way to minimize this is by constructing so-called *surrogate models* which, instead of using approximate physics or phenomenological formulae, rather interpolate within the space of numerical relativity waveforms. In this work, we introduce **NRSurNN3dq4**, a surrogate model for non-precessing BBH merger waveforms powered by neural networks. By relying on the power of deep learning, this approximant is remarkably fast and competitively accurate, as it can generate millions of waveforms in a tenth of a second, while mismatches with numerical relativity waveforms are restrained below 10^{-3} . We implement this approximant within the BILBY framework for gravitational-wave parameter inference, and show that it is suitable for parameter estimation tasks.

I. INTRODUCTION

Gravitational-wave (GW) astronomy is a computationally intensive field. Within the LIGO-Virgo-KAGRA (LVK) collaboration [1–3], a number of detection pipelines (GstLAL [4], MBTA [5], PyCBC [6], SPIIR [7], and cWB [8]) are constantly monitoring detector data in order to inform collaboration members of potential GW signatures, as well as facilitate public alerts for the broader astrophysical community. If a GW trigger is detected by the pipelines of the LVK collaboration, a further analysis is often desired for parameter estimation. In the case of binary black hole (BBH) events, this is done by maximizing some likelihood function based on a similarity metric between the detector data and simulated GW waveforms, typically a noise-weighted inner product, which should reach a maximum if the original wave is exactly the same as some produced simulation [9]. This means one must have at hand some process which, given some physical parameters as input, will produce a physically accurate waveform, while being fast enough to allow an exploration of the GW parameter space. Waveforms from full numerical relativity simulations, which can take weeks to complete, are not appropriate for this task. Instead, one typically uses *approximants*, com-

putational routines which produce fast approximations of what a gravitational waveform should look like given some physical parameters. As they are ultimately tested against (and often calibrated according to) numerical relativity waveform catalogues (such as the ones produced by the SXS collaboration [10]), approximants tend to be highly accurate and indeed have allowed for the analysis of all GW signals detected to date [11–14].

Despite this remarkable success, there is still room for improvement in the field. Parameter estimation is typically done through Bayesian inference based on dynamic nested sampling [15]. This process can be parallelized in order to speed up inference times (note, however, that this speedup is not linear with the number of cores [16]). This is usually done by sending Bayesian inference jobs to high-performance computing (HPC) clusters, making use of large numbers of CPU cores to obtain the desired parallelization gains. However, even for these implementations the computational bottleneck can be found in the calculation of the likelihood, in particular the generation of the waveform.

Next generation GW detectors, namely Einstein Telescope and Cosmic Explorer, are expected to achieve detection rates of 100,000 BBH events per year [17, 18]. In order to process these events efficiently with Bayesian methods, the waveform generation process must be made faster, while still allowing for an accurate parameter estimation. In order to address this issue, applications of deep learning methods to steps of this process have been

*Electronic address: osgrade@alumni.uv.es

proposed. Approaches based on likelihood-free inference avoid the waveform generation step altogether by replacing Bayesian parameter estimation with neural posterior estimation [19], while others strive for a speed-up through more efficient sampling using normalizing flows [20, 21].

In this paper, we instead tackle the problem through the lens of speeding up waveform generation. Existing literature has shown machine learning to be an effective method for waveform generation, in particular to provide reduced order models of existing approximants. These typically involve some sort of low-dimensional representation of the waveform, such as singular value decomposition (SVD), principal component analysis (PCA) or autoencoder bases [22–28]. In this work, we expand on previous work by producing a surrogate model trained directly on numerical relativity data. We introduce `NRSurNN3dq4`¹, a fast and accurate surrogate to the dominant (2,2) mode of numerical-relativity-produced GWs leveraging the GPU-based nature of modern machine learning. By training a small neural network to predict the coefficients of a reduced PCA basis of approximant waveforms, and then fine-tuning on numerical relativity waveforms, we obtain a model which is capable of generating millions of accurate waveforms on a consumer-level GPU in a matter of milliseconds.

The paper is organized as follows: in Section II, we introduce the datasets used in this work, including the approximant and numerical relativity waveforms. Section III describes our methodology, detailing the dimensionality reduction approach and neural network architecture used for training. The results of our model, including accuracy, speed, and parameter estimation capabilities, are presented in Section IV. Finally, we summarize our findings and discuss potential future directions in Section V.

II. DATASETS

In the development of deep learning methods, data availability often poses a significant constraint. This proves particularly problematic in the field of numerical relativity, where the high costs associated with simulations result in a scarcity of data. For instance, by applying constraints of an effective precessing spin $\chi_p < 0.05$ and a mass ratio $q < 6$ to the SXS BBH data [10], we obtain only 381 samples of numerical relativity simulations. Given that deep learning frameworks typically need very large datasets in order to properly interpolate between the points of the input and output parameter spaces, current numerical catalogues are inadequate to fully explore

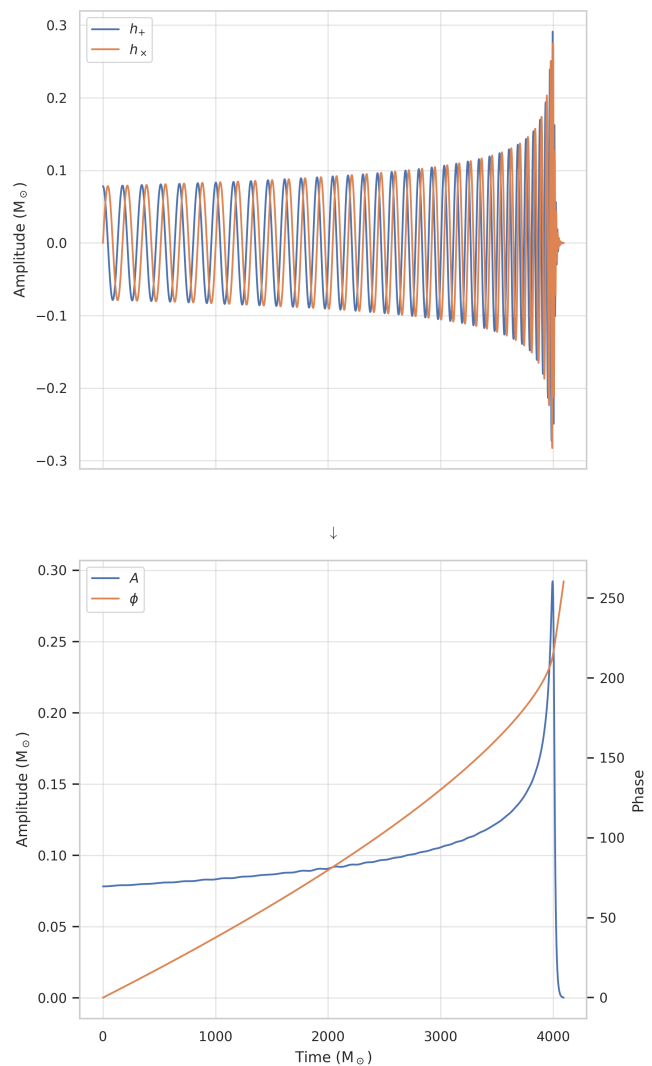


FIG. 1: An example of a BBH waveform generated using the approximant, in the polarization (top) and amplitude-phase (bottom) representations.

them. To compensate for this, we propose to generate a substantial GW dataset using an existing approximant to train a model which can capture the fundamental characteristics of BBH GW signals, and subsequently fine-tune this model using numerical relativity data.

A. Approximant dataset

With the aid of the `GWSURROGATE` package for python [29], we make use of the `NRSur7dq4` surrogate model [30] in order to generate 1,024,000 waveforms. We restrict ourselves to aligned-spin BBH mergers, in order to keep complexity manageable, with mass ratios

¹ The `NRSurNN3dq4` model name indicates its development as a neural network-powered surrogate (NN) trained for non-precessing systems (3d, as the parameter space is fully defined by 3 parameters) with mass ratios up to 4 (q4)

sampled uniformly from the $[1, 6]$ interval², while the aligned (dimensionless) component spins χ_1, χ_2 are sampled uniformly from the $[-0.99, 0.99]$ interval. We note that while uniform sampling does not necessarily reflect population-informed priors, it avoids biasing towards any particular parameter combination. The waveforms are generated in dimensionless (simulation) units, with amplitude and time scaled by the solar mass, with a sample rate of $2 M_\odot^{-1}$. The merger time is estimated as the time which maximizes the amplitude of the quadrupolar $(l, |m|) = (2, 2)$ mode, and the waveforms are trimmed to a duration of $4096 M_\odot$, lining up the merger $100 M_\odot$ before the end of the window. We further simplify our problem by setting the initial phase of the $(2, 2)$ mode in all the waveforms to zero. The $(2, 2)$ mode of the waveform is then saved to an HDF5 file, along with the physical parameters for the generation.

B. Numerical Relativity waveforms

For setting up the numerical relativity dataset, we make use of the publicly available BBH simulation data from the SXS collaboration [10], consisting of 2018 simulations. The $(2, 2)$ waveforms are extracted using the SXS python package [31]. To match the data we produced with the approximant, we must do a number of checks. First, we take into account only the waveforms which have a duration of at least $4096 M_\odot$. Then, we select the non-precessing waveforms by filtering effective precessing spins $\chi_p < 0.05$ [32], with mass ratios $q < 6$, so that we are in line with the approximant data described previously. This process leaves us with only 381 waveforms. These waveforms are interpolated using cubic splines to the same sample rate as the approximant dataset, and trimmed to $4096 M_\odot$.

III. METHODS

A. Dimensionality reduction

When dealing with numerical data, gravitational waveform modes are essentially arrays of M -length complex numbers. They are then, formally speaking, points in \mathbb{C}^M . Taking $N = 2M$, we can reframe this as points in \mathbb{R}^N . However, the high correlation between adjacent points in the waveform, as well as restrictions to the shape of the waveforms (that is, wavelike signals with a chirp and ringdown-like features) means that gravitational waveforms occupy a very restricted subspace of

\mathbb{R}^N . On the other hand, neural networks with N outputs will output to some generic subspace of \mathbb{R}^N , the size of which will depend on the number of layers and neurons per layer (that is, its expressivity). Therefore, we need the network to learn not only the shape of the subspace, as well as how this space is connected. Furthermore, the average Euclidean distance between two points in a cube of side l in \mathbb{R}^N scales as $O(\sqrt{N})$ [33]. This means that, in general, high dimensional data will

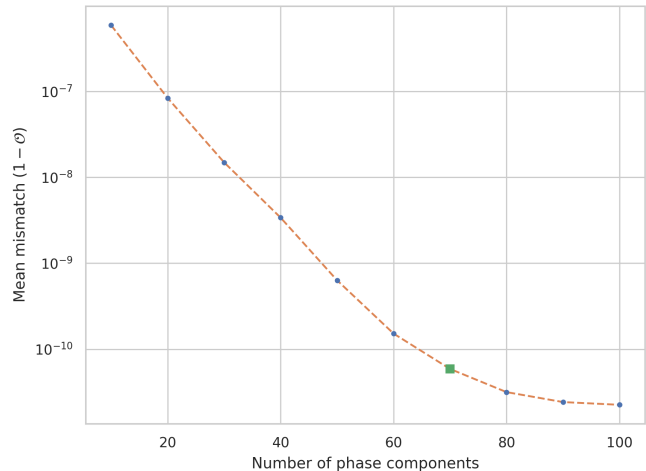


FIG. 2: Mean mismatch values as a function of the number of principal components kept for the phase.

be more sparse than lower dimensional data. As such, a neural network will have to interpolate over longer distances in such a case, which may lead to problems with convergence and generalisation [34]. Therefore, the projection of N -dimensional data to some lower-dimensional space should make the data more dense and thus facilitate the ease of convergence of neural networks training on that data. This is the concept of dimensionality reduction, and it is widely used across applications of machine learning [35–37]. There are many methods for dimensionality reduction, both linear and non-linear. Our use case involves training a model in a lower-dimensional representation space of gravitational waves, and then performing an inverse transform from that space back to the typical waveform representation. This requires that any method we choose must have an accurate inverse transform. While linear methods typically have an easily calculable inverse, non-linear methods very often do not have a tractable inverse, and they must be fitted to the data in a similar way as the forward transform, such as in autoencoders or UMAP [38, 39]. In this work, we will focus on principal component analysis (PCA), one of the most successful linear dimensionality reduction methods [40, 41].

PCA works by calculating a linear transform $\mathcal{L} : X \rightarrow (X - \mu)V$, where X is some input $N \times M$ matrix (interpreted in our case as being a collection of N waveforms of length M), μ is the average value at each timestep, and

² Note that the approximant was trained in the $[1, 4]$ interval, but the creators support generation up to $q = 6$, claiming acceptable accuracy. As such it makes sense to train our model up to this value as well.

V is the $m \times n$ matrix of eigenvectors of the covariance matrix $\Sigma = \frac{1}{n}(X - \mu)^T(X - \mu)$. The crucial point here is that the centering of X means that the eigenvalues of Σ represent the explained variance of the corresponding eigenvector. As such, if we consider only the eigenvalue-sorted subset of the top-valued k eigenvectors, V_k (an $m \times k$ matrix), we can approximately reconstruct the original dataset as

$$X' = [(X - \mu)V_k]V_k^T + \mu. \quad (1)$$

This will have some error E associated to it, which will depend on the amount of components truncated (that is, $E \rightarrow 0$ as $k \rightarrow n$).

In our case, we will separate the complex waveform arrays $h = h_+ - ih_\times = Ae^{i\phi}$ into 2-channel arrays, separating the amplitude A and (unwrapped) phase ϕ quantities, as represented in Figure 1. This allows for a simpler, numerically non-oscillating representation, and also allows us to perform PCA separately on each quantity. Therefore, we can tune the amount of precision required in the reconstruction of each quantity. Specifically, we know that minimizing the error in the phase reconstruction is paramount for a waveform generator which is intended to be used in GW astronomy. Figure 2 shows the average mismatch values (see definition below) as a function of the number of principal components kept for the phase. Going forward, our chosen representation will keep 30 components for the amplitude and 70 components for the phase, thus reducing the 2048-dimensional complex representation of waveforms (which is equivalent to a 4096-dimensional representation) to a 100-dimensional one.

B. Network architecture and training

Conceptually, we propose to build a neural network that maps the 3 physical input parameters (mass ratio and dimensionless individual spins) to the 100-dimensional orthogonal space corresponding to the chosen PCA bases. We can then apply the inverse PCA transform and obtain the reconstructed waveform h . With this formulation, we can now define our optimization objective, or loss function. On the one hand, we want to ensure the accuracy of the predicted PCA components. This can be quantified using a mean absolute error (MAE) criterion,

$$L_1(c, \hat{c}) = \frac{1}{N} \sum_{i=1}^N |c_i - \hat{c}_i|, \quad (2)$$

where c is the generated array of the 100 PCA components for each generated waveforms, and \hat{c} represents the corresponding ground truth values of these components. We choose to use MAE rather than its square as it is more robust to outliers. On the other hand, from a practical perspective, we eventually want to maximize the overlap \mathcal{O} between the waveforms themselves, as that is

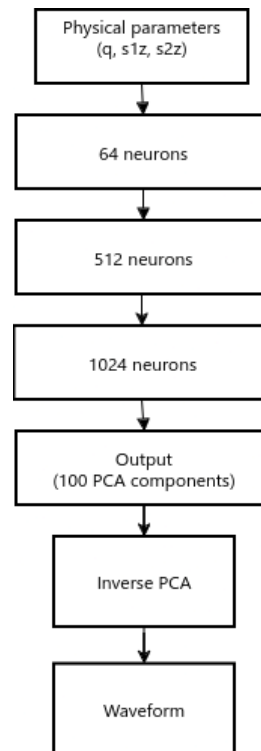


FIG. 3: Visualisation of model architecture.

the usual evaluation metric for approximants. It should be useful, then, to make sure our loss function includes information about the overlap. Note that since we want to *maximize* the overlap, we should then *minimize* the mismatch, given by

$$L_2(h, \hat{h}) = 1 - \mathcal{O}(h, \hat{h}) = 1 - \frac{\langle h | \hat{h} \rangle}{\sqrt{\langle h | h \rangle \langle \hat{h} | \hat{h} \rangle}}, \quad (3)$$

where

$$\begin{aligned} \langle h | \hat{h} \rangle &= 4 \operatorname{Re} \int_{f_{\text{low}}}^{f_{\text{high}}} \tilde{h}(f) \tilde{h}^*(f) df \\ &\approx 4 \operatorname{Re} \sum_k \tilde{h}_k \tilde{h}_k^* \Delta f \end{aligned}$$

is the inner product between waveforms. However, it is more convenient to work with the base-10 logarithm of this quantity, as this will keep the magnitude of the loss (and gradients) more consistent as the mismatch reaches lower values. As such, our loss function \mathcal{L} shall be

$$\mathcal{L} = L_1 + \log(L_2). \quad (4)$$

The network used is a simple multi-layered perceptron with 3 hidden layers, with 64, 512 and 1024 neurons, respectively. The model architecture is illustrated in Figure 3. In this work, all computations make use of the NVIDIA V100 32GB GPU nodes provided by the

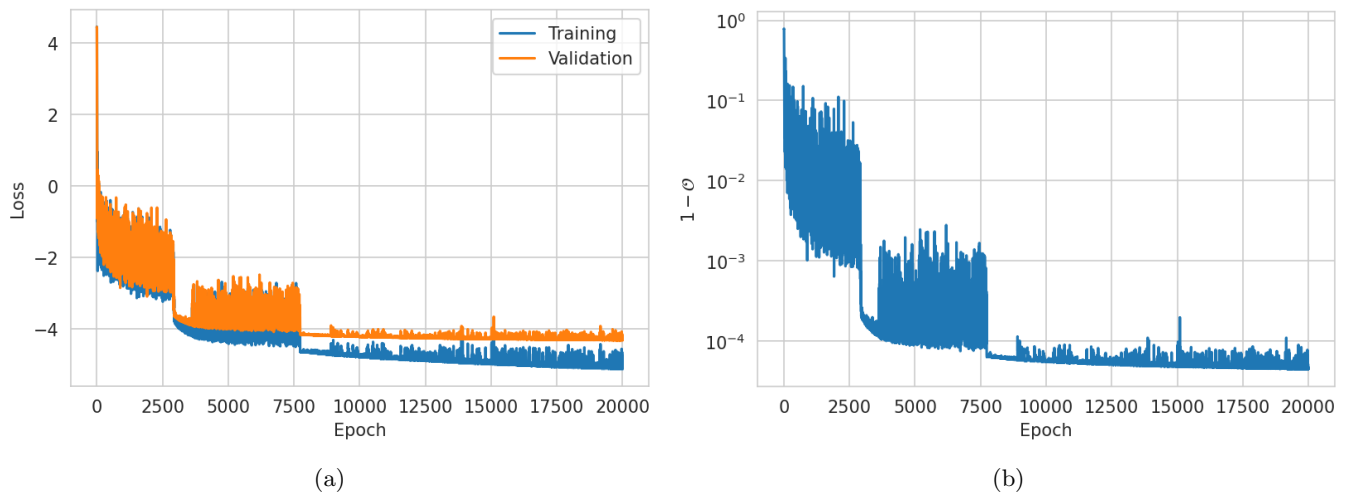


FIG. 4: (a) Training and validation loss on the approximant dataset and, (b) validation mismatches on the approximant dataset.

Artemisa cluster at the University of València. The number and width of the hidden layers are the result of an optimization process through the OPTUNA package [42] (note that in the case of the layer width, we optimized over powers of 2, in order to reduce redundancy). The model is then pre-trained for 20,000 epochs in the approximant dataset, with an 80/20 train/validation split. We use the Sophia optimizer [43], with an initial learning rate of 3×10^{-3} (obtained through the learning rate finder process outlined in [44]), and a learning rate scheduler reducing the learning rate by a factor of 4 after 1000 epochs without improved performance on the validation set. During the training loop we monitor the mean value of the validation mismatches, and save the model every time there is an improvement (that is, when the mean validation mismatch decreases in comparison to the previous best value), guaranteeing we have the best performing model on the training set after all epochs are done. This model will then be fine-tuned on the numerical relativity data. Since the numerical relativity dataset is quite small, we proceed as follows: first, we set apart 1/8th of the waveforms for testing purposes. With the remaining waveforms, we use k-fold cross validation by splitting the data in 5 equal-sized subsets of “folds”. For each iteration, we consider the non-chosen folds as a training set, and the chosen fold as the validation. This allows us to have 5 iterations of training, using the model trained in the approximant as a starting point, and using a lower learning rate than in the pre-training step (1×10^{-4}) in order to avoid an excessive deviation from the region of the space of network weights arrived at in pre-training. When this process is completed, the weights of the 5 trained models are averaged to obtain a final model, which is then evaluated on the test set. This process should be seen as a sort of weight averaging, which has been shown to lead to improved generalization performance [45].

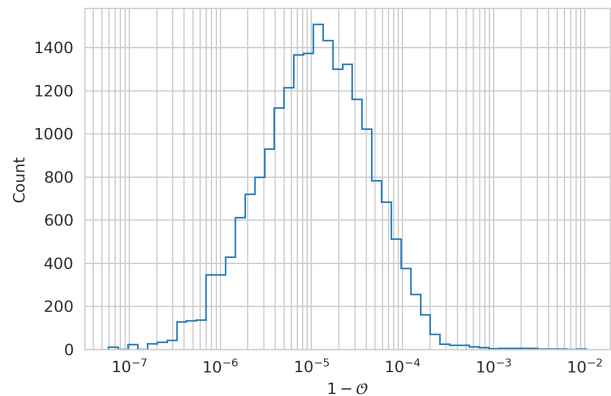


FIG. 5: Distribution of validation mismatches for the model trained on the approximant dataset.

IV. RESULTS

A. Accuracy

1. Results on the approximant waveforms

Figure 4a shows the evolution of the loss function on the training and validation sets as the model trains. We can see that the training loss has some moments of rapid drops, but otherwise decreases steadily. The validation loss follows this same pattern for about the first 7500 epochs, but then starts to plateau, showing very minor improvements until the end. Correspondingly Fig. 4b shows the evolution of the mismatches on the validation set. The lowest mean validation mismatch is achieved at epoch 19910, and as such the final saved model state corresponds to this epoch.

	Fold 0	Fold 1	Fold 2	Fold 3	Fold 4	Avg. Weights	No fine-tuning
Mean mismatch	5.57×10^{-3}	6.50×10^{-3}	5.72×10^{-3}	5.81×10^{-3}	7.15×10^{-3}	5.43×10^{-3}	2.09×10^{-2}
Max mismatch	2.57×10^{-2}	4.39×10^{-2}	2.16×10^{-2}	2.92×10^{-2}	3.16×10^{-2}	2.10×10^{-2}	1.32×10^{-1}

TABLE I: Mean and maximum mismatch values for the various models in the set-aside test set

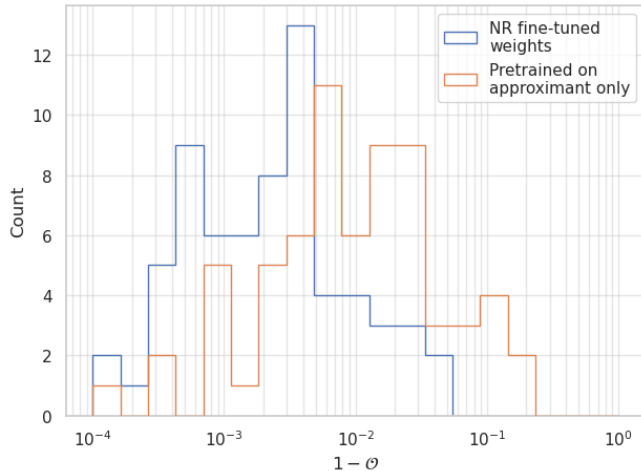


FIG. 6: Distribution of mismatches on the set-aside test dataset, shown for the fine-tuned and weight-averaged final model, as well as for the model trained only on the approximant.

In Fig. 5 we depict the distribution of the mismatch metric on the validation set after pretraining on the approximant dataset. The distribution is peaked around 10^{-5} , with the worst mismatch found in the validation set being 9.5×10^{-3} . This indicates that our network does a good job as a surrogate model of the `NRSur7dq4` approximant under the parameter restrictions of our setup.

2. Results on the Numerical Relativity waveforms

Table I shows the mean and maximum mismatch values for the various trained models in the set-aside test set, including a model trained only on the approximant, before fine-tuning. We can see that the weight averaging of the 5 models trained on the folds results in better mismatches compared to models trained on each individual fold. We can also see that skipping the fine-tuning step (last column) results in mismatches an order of magnitude larger than the fine-tuned models, as further made evident in Figure 6. This makes it clear that the fine-tuning step is crucial to obtain a good numerical relativity surrogate with our methodology.

It is also necessary to point out that the results on the numerical relativity data are worse than the results on the approximant data alone. This may be explained by the increased complexity of the numerical relativity

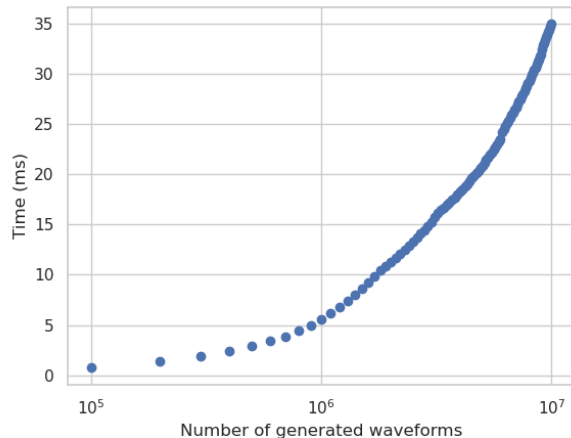


FIG. 7: Cumulative waveform generation time for `NRSurNN3dq4`.

waveforms, as well as by the relatively small amount of data available. Nonetheless, the model is still accurate enough for parameter estimation, as we shall show in Section IV C.

B. Speed

To test the runtime performance of the model, we generate 1×10^7 randomly sampled waveforms in batches of 1×10^5 using an NVIDIA V100 GPU. Note that in this process we are now including the scaling from geometric to physical units. Figure 7 shows the cumulative time taken by `NRSurNN3dq4` to generate the waveforms. We must note here that there is a warm-up period, typically around 500 milliseconds of overhead, attributable to CUDA initialization. However, once initialized, the total generation time for 10^7 waveforms is achieved in under 40 milliseconds.

Figure 8 presents a box plot of the generation time for sets of 20 batches of size 10^2 to 10^5 . As may be expected, as long as GPU memory is not exceeded, the batch size does not significantly affect the mean generation time. This means that approximants in the vein of `NRSurNN3dq4` can be used to generate massive GW template banks in very short time frames.

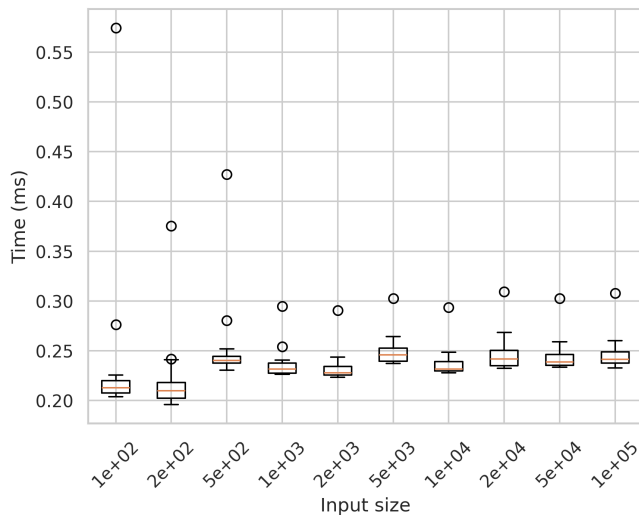


FIG. 8: Box plot showing waveform generation time as a function of input (batch) size. The orange line within each box represents the median time. The box itself shows the interquartile range (IQR), while the whiskers extend to the minimum and maximum times within 1.5 times the IQR. Outliers are shown as individual circles

C. Parameter estimation

As a way of exploring the ability of `NRSurNN3dq4` to be used in parameter estimation pipelines, we here discuss a basic test we conducted using the `BILBY` software suite for GWs [15]. We must note that the current sampler and likelihood implementations in `BILBY` do not allow us at this point to take advantage of CUDA parallelization of the likelihood (though it is in principle possible to write a custom sampler that would manage this). Therefore, we will be running the model in the CPU for this section, focusing mostly on the accuracy of the model for parameter estimation. For comparison’s sake, running the model in CPU mode, it takes us 103 ms to generate a 1000 waveforms in serial. On the other hand, in the same machine, it takes us 810 ms seconds to generate 1000 waveforms with `NRSur7dq4`.

For this experiment, we will focus on performing a parameter inference run on the GW200311_115853 event from the third Gravitational-Wave Transient Catalog [14], using the `NESSAI` sampler [20] and `NRSurNN3dq4` as the waveform model. This model was chosen as an illustrative example due to its relatively high SNR, but performance in other events can be expected to be similar. With 300 live points, this run took 6 minutes and 2 seconds to complete, with 390,704 likelihood evaluations accounting for 39.5 seconds of that time. In Fig. 9 we show the results of the PE run, with the posteriors being calculated for the mass ratio q and the spins χ_1 , χ_2 , as well as the chirp mass $\mathcal{M} = \frac{(m_1 m_2)^{3/5}}{(m_1 + m_2)^{1/5}}$, luminosity distance d_L , the sky position angular coordinates (right

ascension α and declination δ), and the polarization angle Ψ . All estimated values are contained in the 90% credible regions of the LVK posterior distributions, showing that our model can be used to reliably reconstruct physical parameters in line with LVK standards.

V. CONCLUSIONS

In this paper we have introduced `NRSurNN3dq4`, a neural-network-based surrogate model designed to rapidly and accurately generate non-precessing BBH waveforms. By mapping the physical input parameters to a reduced 100-dimensional space of PCA coefficients, our model can reconstruct waveforms with low mismatches. The initial results on approximant data show average waveform mismatches of the order of 10^{-5} , yielding immediate promise for these methods as reduced-order models for approximants. While the results after fine-tuning on numerical relativity data are not quite as good as for the case of approximants, likely due to the lack of data, the average numerical relativity waveform mismatches are of the order of 5×10^{-3} . The fact that the fine-tuned model achieves mismatches with numerical relativity waveforms an order of magnitude lower than the pretrained model reinforces the idea that this 2-step training procedure is effective. Crucially, timing tests demonstrate that `NRSurNN3dq4` can generate over a million waveforms in under a tenth of a second when implemented in a GPU. This makes `NRSurNN3dq4` a powerful tool when the generation of large amounts of waveforms in parallel is required, such as building template banks, building datasets for training machine learning models, or for GPU-parallelized parameter estimation.

The evaluation of this model within the `BILBY` framework shows results that are consistent with those reported in the literature. The results for parameter estimation confirm the model’s accuracy and open the door for further integration. A GPU adaptation of existing `BILBY` samplers and likelihood implementations in order to leverage the ability to generate arbitrarily large numbers of waveforms has the potential to speed up parameter estimation in a very significant way and must be the focus of future work. Additional future efforts could focus on extending the model’s capabilities to precessing systems and higher modes, as well as refining its accuracy through the exploration of alternative dimensionality reduction methods and alternative network architectures.

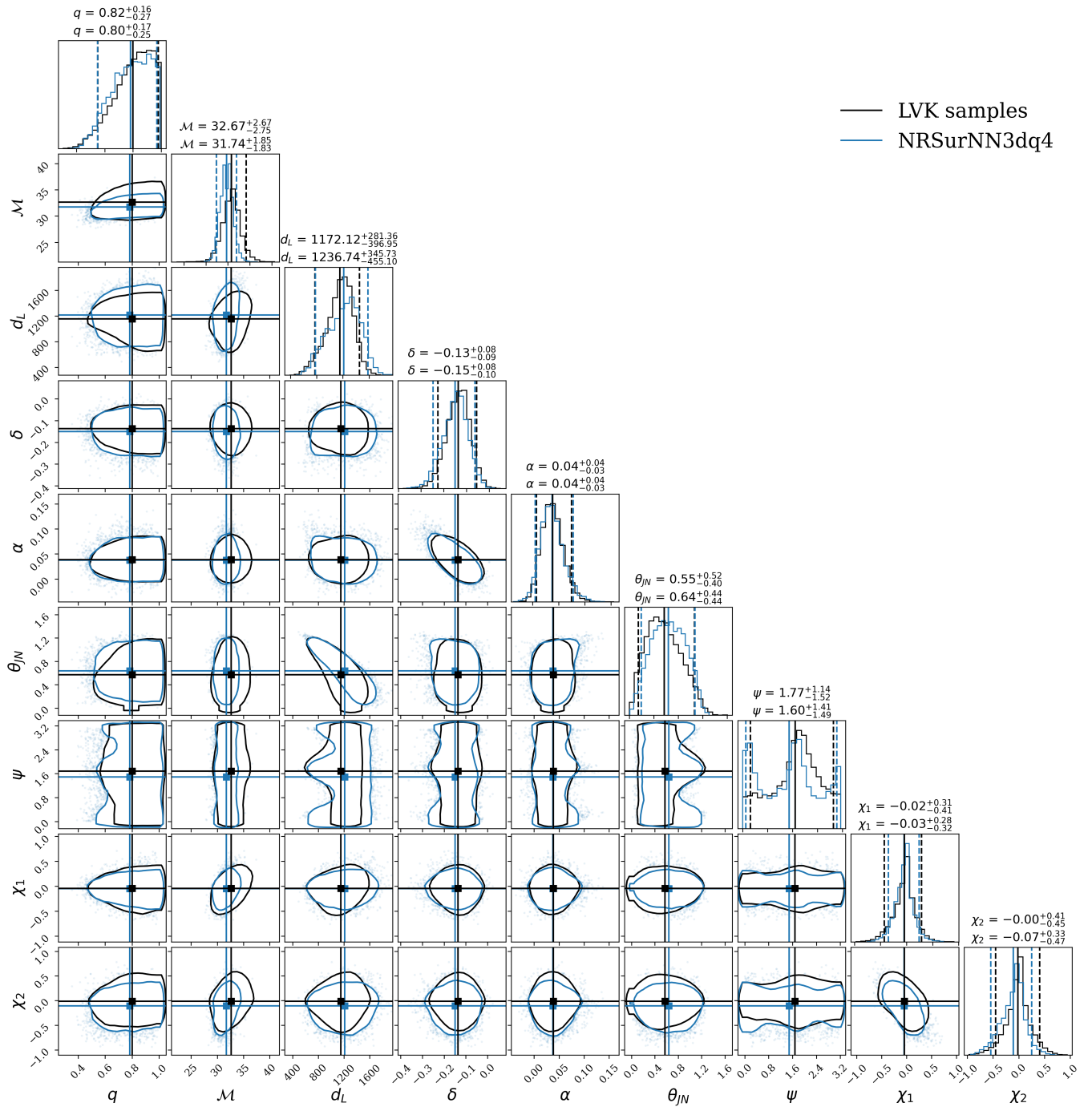


FIG. 9: Corner plot showing the relevant subset of posterior distributions of the BILBY parameter estimation. The dashed lines in the 1D histograms represent the 90% credible intervals, while the isolines in the 2D plots represent the 90% credible regions.

Acknowledgments

OGF is supported by the Portuguese Foundation for Science and Technology (FCT) through doctoral scholarship UI/BD/154358/2022. TF is supported by FCT through doctoral scholarship (reference 2023.03753.BD). OGF, TF, SN and AO ac-

knowledge financial support by CF-UM-UP through Strategic Funding UIDB/04650/2020. JAF and ATF are supported by the Spanish Agencia Estatal de Investigación (PID2021-125485NB-C21) funded by MCIN/AEI/10.13039/501100011033 and ERDF A way of making Europe. Further support is provided by the Generalitat Valenciana (CIPROM/2022/49) and by

the European Horizon Europe staff exchange (SE) programme HORIZON-MSCA-2021-SE-01 (NewFunFiCO-101086251). AO is partially supported by FCT, under the Contract CERN/FIS-PAR/0037/2021. JDMG is partially supported by the agreement funded by the European Union, between the Valencian Ministry of Innovation, Universities, Science and Digital Society, and the network of research centers in Artificial Intelligence (Valencian Foundation valgrAI), as well as the Valencian Government grant with reference number CIAICO/2021/184; the Spanish Ministry of Economic Affairs and Digital Transformation through the QUANTUM ENIA project call – Quantum Spain project, and the European Union through the Recovery, Transformation and Resilience Plan – NextGenerationEU within the framework of the Digital Spain 2025 Agenda. The authors gratefully acknowledge the computer resources at Artemisa and the technical support provided by the Instituto de Fisica Corpuscular, IFIC (CSIC-UV). Artemisa is co-funded by the European Union through the 2014-2020 ERDF Operative Programme of Comunitat Valenciana, project IDIFEDER/2018/048. This material is

based upon work supported by NSF’s LIGO Laboratory which is a major facility fully funded by the National Science Foundation, as well as the Science and Technology Facilities Council (STFC) of the United Kingdom, the Max-Planck-Society (MPS), and the State of Niedersachsen/Germany for support of the construction of Advanced LIGO and construction and operation of the GEO600 detector. Additional support for Advanced LIGO was provided by the Australian Research Council. Virgo is funded, through the European Gravitational Observatory (EGO), by the French Centre National de Recherche Scientifique (CNRS), the Italian Istituto Nazionale di Fisica Nucleare (INFN) and the Dutch Nikhef, with contributions by institutions from Belgium, Germany, Greece, Hungary, Ireland, Japan, Monaco, Poland, Portugal, Spain. KAGRA is supported by Ministry of Education, Culture, Sports, Science and Technology (MEXT), Japan Society for the Promotion of Science (JSPS) in Japan; National Research Foundation (NRF) and Ministry of Science and ICT (MSIT) in Korea; Academia Sinica (AS) and National Science and Technology Council (NSTC) in Taiwan

-
- [1] The LIGO Scientific Collaboration, J Aasi, B P Abbott, R Abbott, T Abbott, M R Abernathy, K Ackley, C Adams, T Adams, P Addresso, R X Adhikari, V Adya, C Affeldt, N Aggarwal, O D Aguiar, A Ain, P Ajith, A Alemic, B Allen, D Amariutei, S B Anderson, W G Anderson, K Arai, M C Araya, C Arceneaux, J S Areeda, G Ashton, S Ast, S M Aston, P Aufmuth, C Aulbert, B E Aylott, S Babak, P T Baker, S W Ballmer, J C Barayoga, M Barbet, S Barclay, B C Barish, D Barker, B Barr, L Barsotti, J Bartlett, M A Barton, I Bartos, R Bassiri, J C Batch, C Baune, B Behnke, A S Bell, C Bell, M Benacquista, J Bergman, G Bergmann, C P L Berry, J Betzwieser, S Bhagwat, R Bhandare, I A Bilenko, G Billingsley, J Birch, S Biscans, C Biwer, J K Blackburn, L Blackburn, C D Blair, D Blair, O Bock, T P Bodiya, P Bojtos, C Bond, R Bork, M Born, Sukanta Bose, P R Brady, V B Braginsky, J E Brau, D O Bridges, M Brinkmann, A F Brooks, D A Brown, D D Brown, N M Brown, S Buchman, A Buikema, A Buonanno, L Cadonati, J Calderón Bustillo, J B Camp, K C Cannon, J Cao, C D Capano, S Caride, S Caudill, M Cavaglià, C Cepeda, R Chakraborty, T Chalermongsak, S J Chamberlin, S Chao, P Charlton, Y Chen, H S Cho, M Cho, J H Chow, N Christensen, Q Chu, S Chung, G Ciani, F Clara, J A Clark, C Collette, L Cominsky, M Constancio, D Cook, T R Corbitt, N Cornish, A Corsi, C A Costa, M W Coughlin, S Countryman, P Couvares, D M Coward, M J Cowart, D C Coyne, R Coyne, K Craig, J D E Creighton, T D Creighton, J Cripe, S G Crowder, A Cumming, L Cunningham, C Cutler, K Dahl, T Dal Canton, M Damjanic, S L Danilishin, K Danzmann, L Dartez, I Dave, H Daveloza, G S Davies, E J Daw, D DeBra, W Del Pozzo, T Denker, T Dent, V Dergachev, R T DeRosa, R DeSalvo, S Dhurandhar, M D’iaz, I Di Palma, G Dojcinoski, E Dominguez, F Donovan, K L Dooley, S Doravari, R Douglas, T P Downes, J C Driggers, Z Du, S Dwyer, T Eberle, T Edo, M Edwards, M Edwards, A Effler, H.-B Eggenstein, P Ehrens, J Eichholz, S S Eikenberry, R Essick, T Etzel, M Evans, T Evans, M Factourovich, S Fairhurst, X Fan, Q Fang, B Farr, W M Farr, M Favata, M Fays, H Fehrmann, M M Fejer, D Feldbaum, E C Ferreira, R P Fisher, Z Frei, A Freise, R Frey, T T Fricke, P Fritschel, V V Frolov, S Fuentes-Tapia, P Fulda, M Fyffe, J R Gair, S Gaonkar, N Gehrels, L Á Gergely’, J A Giaime, K D Giardina, J Gleason, E Goetz, R Goetz, L Gondan, G González, N Gordon, M L Gorodetsky, S Gossan, S Gößler, C Gräf, P B Graff, A Grant, S Gras, C Gray, R J S Greenhalgh, A M Gretarsson, H Grote, S Grunewald, C J Guido, X Guo, K Gushwa, E K Gustafson, R Gustafson, J Hacker, E D Hall, G Hammond, M Hanke, J Hanks, C Hanna, M D Hannam, J Hanson, T Hardwick, G M Harry, I W Harry, M Hart, M T Hartman, C-J Haster, K Haughian, S Hee, M Heintze, G Heinzl, M Hendry, I S Heng, A W Heptonstall, M Heurs, M Hewitson, S Hild, D Hoak, K A Hodge, S E Hollitt, K Holt, P Hopkins, D J Hosken, J Hough, E Houston, E J Howell, Y M Hu, E Huerta, B Hughey, S Husa, S H Huttner, M Huynh, T Huynh-Dinh, A Idrisy, N Indik, D R Ingram, R Inta, G Islas, J C Isler, T Isogai, B R Iyer, K Izumi, M Jacobson, H Jang, S Jawahar, Y Ji, F Jiménez-Forteza, W W Johnson, D I Jones, R Jones, L Ju, K Haris, V Kalogera, S Kandhasamy, G Kang, J B Kanner, E Katsavounidis, W Katzman, H Kaufer, S Kaufer, T Kaur, K Kawabe, F Kawazoe, G M Keiser, D Keitel, D B Kelley, W Kells, D G Keppel, J S Key, A Khalaidovski, F Y Khalili, E A Khazanov, C Kim, K Kim, N G Kim, N Kim, Y.-M Kim, E J King, P J King, D L Kinzel, J S Kissel, S Klimenko, J Kline, S Koehlenbeck, K Kokeyama, V Kondrashov,

- M Korobko, W Z Korth, D B Kozak, V Kringel, B Krishnan, C Krueger, G Kuehn, A Kumar, P Kumar, L Kuo, M Landry, B Lantz, S Larson, P D Lasky, A Lazzarini, C Lazzaro, J Le, P Leaci, S Leavey, E O Lebigot, C H Lee, H K Lee, H M Lee, J R Leong, Y Levin, B Levine, J Lewis, T G F Li, K Libbrecht, A Libson, A C Lin, T B Littenberg, N A Lockerbie, V Lockett, J Logue, A L Lombardi, M Lormand, J Lough, M J Lubinski, H Lück, A P Lundgren, R Lynch, Y Ma, J Macarthur, T MacDONald, B Machenschalk, M MacInnis, D M Macleod, F Magaña-Sandoval, R Magee, M Mageswaran, C Maglione, K Mairland, I Mandel, V Mandic, V Mangano, G L Mansell, S Márka, Z Márka, A Markosyan, E Maros, I W Martin, R M Martin, D Martynov, J N Marx, K Mason, T J Massinger, F Matichard, L Matone, N Mavalvala, N Mazumder, G Mazzolo, R McCarthy, D E McClelland, S McCormick, S C McGuire, G McIntyre, J McIver, K McLin, S McWilliams, G D Meadors, M Meinders, A Melatos, G Mendell, R A Mercer, S Meshkov, C Messenger, P M Meyers, H Miao, H Middleton, E E Mikhailov, A Miller, J Miller, M Millhouse, J Ming, S Mirshekari, C Mishra, S Mitra, V P Mitrofanov, G Mitselmakher, R Mittleman, B Moe, S D Mohanty, S R P Mohapatra, B Moore, D Moraru, G Moreno, S R Morriss, K Mossavi, C M Mow-Lowry, C L Mueller, G Mueller, S Mukherjee, A Mullavey, J Munch, D Murphy, P G Murray, A Mytidis, T Nash, R K Nayak, V Necula, K Nedkova, G Newton, T Nguyen, A B Nielsen, S Nisanke, A H Nitz, D Nolting, M E N Normandin, L K Nuttall, E Ochsner, J O'Dell, E Oelker, G H Ogin, J J Oh, S H Oh, F Ohme, P Oppermann, R Oram, B O'Reilly, W Ortega, R O'Shaughnessy, C Osthelder, C D Ott, D J Ottaway, R S Ottens, H Overmier, B J Owen, C Padilla, A Pai, S Pai, O Palashov, A Pal-Singh, H Pan, C Pankow, F Pannarale, B C Pant, M A Papa, H Paris, Z Patrick, M Pedraza, L Pekowsky, A Pele, S Penn, A Perreca, M Phelps, V Pierro, I M Pinto, M Pitkin, J Poeld, A Post, A Poteomkin, J Powell, J Prasad, V Predoi, S Premachandra, T Prestegard, L R Price, M Principe, S Privitera, R Prix, L Prokhorov, O Puncken, M Pürner, J Qin, V Quetschke, E Quintero, G Quiroga, R Quitzow-James, F J Raab, D S Rabeling, H Radkins, P Raffai, S Raja, G Rajalakshmi, M Rakhmanov, K Ramirez, V Raymond, C M Reed, S Reid, D H Reitze, O Reula, K Riles, N A Robertson, R Robie, J G Rollins, V Roma, J D Romano, G Romanov, J H Romie, S Rowan, A Rüdiger, K Ryan, S Sachdev, T Sadecki, L Sadeghian, M Saleem, F Salemi, L Sammut, V Sandberg, J R Sanders, V Sannibale, I Santiago-Prieto, B S Sathyaprakash, P R Saulson, R Savage, A Sawadsky, J Scheuer, R Schilling, P Schmidt, R Schnabel, R M S Schofield, E Schreiber, D Schuette, B F Schutz, J Scott, S M Scott, D Sellers, A S Sengupta, A Sergeev, G Serna, A Sevigny, D A Shaddock, M S Shahriar, M Shaltev, Z Shao, B Shapiro, P Shawhan, D H Shoemaker, T L Sidery, X Siemens, D Sigg, A D Silva, D Simakov, A Singer, L Singer, R Singh, A M Sintes, B J J Slagmolen, J R Smith, M R Smith, R J E Smith, N D Smith-Lefebvre, E J Son, B Sorazu, T Souradeep, A Staley, J Stebbins, M Steinke, J Steinlechner, S Steinlechner, D Steinmeyer, B C Stephens, S Stepleski, S Stevenson, R Stone, K A Strain, S Strigin, R Sturani, A L Stuver, T Z Summerscales, P J Sutton, M Szczepanczyk, G Szeifert, D Talukder, D B Tanner, M Tápai, S P Tarabrin, A Taracchini, R Taylor, G Tellez, T Theeg, M P Thiruganasambandam, M Thomas, P Thomas, K A Thorne, K S Thorne, E Thrane, V Tiwari, C Tomlinson, C V Torres, C I Torrie, G Traylor, M Tse, D Tshilumba, D Ugolini, C S Unnikrishnan, A L Urban, S A Usman, H Vahlbruch, G Vajente, G Valdes, M Vallisneri, A A van Veggel, S Vass, R Vaulin, A Vecchio, J Veitch, P J Veitch, K Venkateswara, R Vincent-Finley, S Vitale, T Vo, C Vorvick, W D Vousden, S P Vyatchanin, A R Wade, L Wade, M Wade, M Walker, L Wallace, S Walsh, H Wang, M Wang, X Wang, R L Ward, J Warner, M Was, B Weaver, M Weinert, A J Weinstein, R Weiss, T Welborn, L Wen, P Wessels, T Westphal, K Wette, J T Whelan, S E Whitcomb, D J White, B F Whiting, C Wilkinson, L Williams, R Williams, A R Williamson, J L Willis, B Willke, M Wimmer, W Winkler, C C Wipf, H Wittel, G Woan, J Worden, S Xie, J Yablon, I Yakushin, W Yam, H Yamamoto, C C Yancey, Q Yang, M Zanolin, Fan Zhang, L Zhang, M Zhang, Y Zhang, C Zhao, M Zhou, X J Zhu, M E Zucker, S Zuraw, and J Zweigig. *Advanced ligo. Classical and Quantum Gravity*, 32(7):074001, mar 2015.
- [2] F Acernese, M Agathos, K Agatsuma, D Aisa, N Allemandou, A Allocca, J Amarni, P Astone, G Balestri, G Ballardin, F Barone, J-P Baronick, M Barsuglia, A Basti, F Basti, Th S Bauer, V Bavigadda, M Bejger, M G Beker, C Belczynski, D Bersanetti, A Bertolini, M Bitossi, M A Bizouard, S Bloemen, M Blom, M Boer, G Bogaert, D Bondi, F Bondu, L Bonelli, R Bonnard, V Boschi, L Bosi, T Bouedo, C Bradaschia, M Branchesi, T Briant, A Brillet, V Brisson, T Bulik, H J Bulten, D Buskulic, C Buy, G Cagnoli, E Calloni, C Campeggi, B Canuel, F Carbognani, F Cavalier, R Cavalieri, G Cella, E Cesarini, E Chassande-Mottin, A Chincarini, A Chiummo, S Chua, F Cleva, E Coccia, P-F Cohadon, A Colla, M Colombini, A Conte, J-P Coulon, E Cuoco, A Dalmaz, S D'Antonio, V Dattilo, M Davier, R Day, G Debreczeni, J Degallaix, S Deléglise, W Del Pozzo, H Dereli, R De Rosa, L Di Fiore, A Di Lieto, A Di Virgilio, M Doets, V Dolique, M Drago, M Ducrot, G Endrőczy, V Fafone, S Farinon, I Ferrante, F Ferrini, F Fiducario, I Fiori, R Flaminio, J-D Fournier, S Franco, S Frasca, F Frasconi, L Gammaitoni, F Garufi, M Gaspard, A Gatto, G Gemme, B Genre, E Genin, A Gennai, S Ghosh, L Giacobone, A Giazotto, R Gouaty, M Granata, G Greco, P Groot, G M Guidi, J Harms, A Heidmann, H Heitmann, P Hello, G Hemming, E Hennes, D Hofman, P Jananowski, R J G Jonker, M Kasprzack, F Kéfélian, I Kowalska, M Kraan, A Królak, A Kutynia, C Lazzaro, M Leonardi, N Leroy, N Letendre, T G F Li, B Lieunard, M Lorenzini, V Loriette, G Losurdo, C Magazzù, E Majorana, I Maksimovic, V Malvezzi, N Man, V Mangano, M Mantovani, F Marchesoni, F Marion, J Marque, F Martelli, L Martellini, A Masserot, D Meacher, J Meidam, F Mezzani, C Michel, L Milano, Y Minenkov, A Moggi, M Mohan, M Montani, N Morgado, B Mours, F Mul, M F Nagy, I Nardecchia, L Naticchioni, G Nelemans, I Neri, M Neri, F Nocera, E Pacaud, C Palomba, F Paoletti, A Paoli, A Pasqualetti, R Passaquieti, D Passuello, M Perciballi, S Petit, M Pichot, F Piergiovanni, G Piliant, A Piluso, L Pinard, R Poggiani, M Prijatelj, G A Prodi, M Punturo, P Puppó, D S Rabeling, I Rácz,

- P Rapagnani, M Razzano, V Re, T Regimbau, F Ricci, F Robinet, A Rocchi, L Rolland, R Romano, D Rosińska, P Ruggi, E Saracco, B Sassolas, F Schimmel, D Sentenac, V Sequino, S Shah, K Siellez, N Straniero, B Swinkels, M Tacca, M Tonelli, F Travasso, M Turconi, G Vajente, N van Bakel, M van Beuzekom, J F J van den Brand, C Van Den Broeck, M V van der Sluys, J van Heijningen, M Vasúth, G Vedovato, J Veitch, D Verkindt, F Vetrano, A Viceré, J-Y Vinet, G Visser, H Vocca, R Ward, M Was, L-W Wei, M Yvert, A Zadro žny, and J-P Zendri. Advanced virgo: a second-generation interferometric gravitational wave detector. *Classical and Quantum Gravity*, 32(2):024001, dec 2014.
- [3] T. Akutsu, M. Ando, K. Arai, Y. Arai, S. Araki, A. Araya, N. Aritomi, H. Asada, Y. Aso, S. Atsuta, K. Awai, S. Bae, L. Baiotti, M. A. Barton, K. Cannon, E. Capocasa, C-S. Chen, T-W. Chiu, K. Cho, Y-K. Chu, K. Craig, W. Creus, K. Doi, K. Eda, Y. Enomoto, R. Flaminio, Y. Fujii, M.-K. Fujimoto, M. Fukunaga, M. Fukushima, T. Furuhata, S. Haino, K. Hasegawa, K. Hashino, K. Hayama, S. Hirobayashi, E. Hirose, B. H. Hsieh, C-Z. Huang, B. Ikenoue, Y. Inoue, K. Ioka, Y. Itoh, K. Izumi, T. Kaji, T. Kajita, M. Kakizaki, M. Kamiizumi, S. Kanbara, N. Kanda, S. Kanemura, M. Kaneyama, G. Kang, J. Kasuya, Y. Kataoka, N. Kawai, S. Kawamura, T. Kawasaki, C. Kim, J. Kim, J. C. Kim, W. S. Kim, Y.-M. Kim, N. Kimura, T. Kinugawa, S. Kirii, Y. Kitaoka, H. Kitazawa, Y. Kojima, K. Kokeyama, K. Komori, A. K. H. Kong, K. Kotake, R. Kozu, R. Kumar, H-S. Kuo, S. Kuroyanagi, H. K. Lee, H. M. Lee, H. W. Lee, M. Leonardi, C-Y. Lin, F-L. Lin, G. C. Liu, Y. Liu, E. Majorana, S. Mano, M. Marchio, T. Matsui, F. Matsushima, Y. Michimura, N. Mio, O. Miyakawa, A. Miyamoto, T. Miyamoto, K. Miyo, S. Miyoki, W. Morii, S. Morisaki, Y. Moriwaki, T. Morozumi, M. Musha, K. Nagano, S. Nagano, K. Nakamura, T. Nakamura, H. Nakano, M. Nakano, K. Nakao, T. Narikawa, L. Naticchioni, L. Nguyen Quynh, W.-T. Ni, A. Nishizawa, Y. Obuchi, T. Ochi, J. J. Oh, S. H. Oh, M. Ohashi, N. Ohishi, M. Ohkawa, K. Okutomi, K. Ono, K. Oohara, C. P. Ooi, S-S. Pan, J. Park, F. E. Peña Arellano, I. Pinto, N. Sago, M. Saijo, S. Saitou, Y. Saito, K. Sakai, Y. Sakai, Y. Sakai, M. Sasai, M. Sasaki, Y. Sasaki, S. Sato, N. Sato, T. Sato, Y. Sekiguchi, N. Seto, M. Shibata, T. Shimoda, H. Shinkai, T. Shishido, A. Shoda, K. Somiya, E. J. Son, A. Suemasa, T. Suzuki, T. Suzuki, H. Tagoshi, H. Tahara, H. Takahashi, R. Takahashi, A. Takamori, H. Takeda, H. Tanaka, K. Tanaka, T. Tanaka, S. Tanioka, E. N. Tapia San Martin, D. Tatsumi, T. Tomaru, T. Tomura, F. Travasso, K. Tsubono, S. Tsuchida, N. Uchikata, T. Uchiyama, T. Uehara, S. Ueki, K. Ueno, F. Uraguchi, T. Ushiba, M. H. P. M. van Putten, H. Vocca, S. Wada, T. Wakamatsu, Y. Watanabe, W-R. Xu, T. Yamada, A. Yamamoto, K. Yamamoto, K. Yamamoto, S. Yamamoto, T. Yamamoto, K. Yokogawa, J. Yokoyama, T. Yokozawa, T. H. Yoon, T. Yoshioka, H. Yuzurihara, S. Zeidler, and Z.-H. Zhu. Kagra: 2.5 generation interferometric gravitational wave detector. *Nature Astronomy*, 3(1):35–40, January 2019.
- [4] Surabhi Sachdev, Sarah Caudill, Heather Fong, Rico K. L. Lo, Cody Messick, Debnandini Mukherjee, Ryan Magee, Leo Tsukada, Kent Blackburn, Patrick Brady, Patrick Brockill, Kipp Cannon, Sydney J. Chamberlin, Deep Chatterjee, Jolien D. E. Creighton, Patrick Godwin, Anuradha Gupta, Chad Hanna, Shasvath Kapadia, Ryan N. Lang, Tjonnie G. F. Li, Duncan Meacher, Alexander Pace, Stephen Privitera, Laleh Sadeghian, Leslie Wade, Madeline Wade, Alan Weinstein, and Sophia Liting Xiao. The gstlal search analysis methods for compact binary mergers in advanced ligo’s second and advanced virgo’s first observing runs, 2019.
- [5] F Aubin, F Brighenti, R Chierici, D Estevez, G Greco, G M Guidi, V Juste, F Marion, B Mours, E Nitoglia, O Sauter, and V Sordini. The mbta pipeline for detecting compact binary coalescences in the third ligo–virgo observing run. *Classical and Quantum Gravity*, 38(9):095004, apr 2021.
- [6] Tito Dal Canton, Alexander H. Nitz, Bhooshan Gadre, Gareth S. Cabourn Davies, Veronica Villa-Ortega, Thomas Dent, Ian Harry, and Liting Xiao. Real-time search for compact binary mergers in advanced ligo and virgo’s third observing run using pycbc live. *The Astrophysical Journal*, 923(2):254, dec 2021.
- [7] Qi Chu, Manoj Kovalam, Linqing Wen, Teresa Slaven-Blair, Joel Bosveld, Yanbei Chen, Patrick Clearwater, Alex Codoreanu, Zhihui Du, Xiangyu Guo, Xiaoyang Guo, Kyungmin Kim, Tjonnie G. F. Li, Victor Oloworaran, Fiona Panther, Jade Powell, Anand S. Sengupta, Karl Wette, and Xingjiang Zhu. The spir online coherent pipeline to search for gravitational waves from compact binary coalescences, 2021.
- [8] S Klimenko, G Vedovato, M Drago, F Salemi, V Tiwari, GA Prodi, C Lazzaro, K Ackley, S Tiwari, CF Da Silva, and G Mitselmakher. Method for detection and reconstruction of gravitational wave transients with networks of advanced detectors. *Physical Review D*, 93(4), February 2016.
- [9] Michele Maggiore. *Gravitational Waves: Volume 1: Theory and Experiments*. Oxford University Press, 10 2007.
- [10] Michael Boyle et al. The SXS collaboration catalog of binary black hole simulations. *Classical and Quantum Gravity*, 36(19):195006, October 2019.
- [11] B. P. Abbott et al. Gwtc-1: A gravitational-wave transient catalog of compact binary mergers observed by ligo and virgo during the first and second observing runs. *Physical Review X*, 9(3), September 2019.
- [12] R. Abbott et al. GWTC-2: Compact Binary Coalescences Observed by LIGO and Virgo During the First Half of the Third Observing Run. *Phys. Rev. X*, 11:021053, 2021.
- [13] R. Abbott et al. GWTC-2.1: Deep Extended Catalog of Compact Binary Coalescences Observed by LIGO and Virgo During the First Half of the Third Observing Run, 8 2021.
- [14] R. Abbott et al. GWTC-3: Compact Binary Coalescences Observed by LIGO and Virgo During the Second Part of the Third Observing Run. *arXiv e-prints*, page arXiv:2111.03606, November 2021.
- [15] Gregory Ashton et al. BILBY: A user-friendly Bayesian inference library for gravitational-wave astronomy. *Astrophys. J. Suppl.*, 241(2):27, 2019.
- [16] W. J. Handley, M. P. Hobson, and A. N. Lasenby. polychord: next-generation nested sampling. *Monthly Notices of the Royal Astronomical Society*, 453(4):4385–4399, September 2015.
- [17] Marica Branchesi, Michele Maggiore, David Alonso, Charles Badger, Biswajit Banerjee, Freija Beirnaert, Enis

- Belgacem, Swetha Bhagwat, Guillaume Boileau, Ssohrab Borhanian, Daniel David Brown, Man Leong Chan, Giulia Cusin, Stefan L. Danilishin, Jerome Degallaix, Valerio De Luca, Arnab Dhani, Tim Dietrich, Ulyana Dupletsa, Stefano Foffa, Gabriele Franciolini, Andreas Freise, Gianluca Gemme, Boris Goncharov, Archisman Ghosh, Francesca Gulminelli, Ish Gupta, Pawan Kumar Gupta, Jan Harms, Nandini Hazra, Stefan Hild, Tanja Hinderer, Ik Siong Heng, Francesco Iacovelli, Justin Janquart, Kamiel Janssens, Alexander C. Jenkins, Chinmay Kalaghatgi, Xhesika Korovesi, Tjonnie G.F. Li, Yufeng Li, Eleonora Loffredo, Elisa Maggio, Michele Mancarella, Michela Mapelli, Katarina Martinovic, Andrea Maselli, Patrick Meyers, Andrew L. Miller, Chiranjib Mondal, Niccolò Muttoni, Harsh Narola, Micaela Oertel, Gor Oganessian, Costantino Pacilio, Cristiano Palomba, Paolo Pani, Antonio Pasqualetti, Albino Perego, Carole Périgois, Mauro Pieroni, Ornella Juliana Piccinni, Anna Puecher, Paola Puppo, Angelo Ricciardone, Antonio Riotto, Samuele Ronchini, Mairi Sakellariadou, Anuradha Samajdar, Filippo Santoliquido, B.S. Sathyaprakash, Jessica Steinlechner, Sebastian Steinlechner, Andrei Utina, Chris Van Den Broeck, and Teng Zhang. Science with the einstein telescope: a comparison of different designs. *Journal of Cosmology and Astroparticle Physics*, 2023(07):068, July 2023.
- [18] Evan D. Hall. Cosmic explorer: A next-generation ground-based gravitational-wave observatory. *Galaxies*, 10(4), 2022.
- [19] Maximilian Dax, Stephen R. Green, Jonathan Gair, Jakob H. Mücke, Alessandra Buonanno, and Bernhard Schölkopf. Real-time gravitational wave science with neural posterior estimation. *Physical Review Letters*, 127(24), December 2021.
- [20] Michael J. Williams, John Veitch, and Chris Messenger. Nested sampling with normalizing flows for gravitational-wave inference. *Phys. Rev. D*, 103(10):103006, 2021.
- [21] Michael J. Williams. nessai: Nested sampling with artificial intelligence, February 2021.
- [22] Sebastian Khan and Rhys Green. Gravitational-wave surrogate models powered by artificial neural networks. *Physical Review D*, 103(6), March 2021.
- [23] Lalit Pathak, Amit Reza, and Anand S. Sengupta. Fast and faithful interpolation of numerical relativity surrogate waveforms using a meshfree approximation. *Phys. Rev. D*, 110:064022, Sep 2024.
- [24] Paraskevi Nousi, Styliani-Christina Fragkouli, Nikolaos Passalis, Panagiotis Iosif, Theocharis Apostolatos, George Pappas, Nikolaos Stergioulas, and Anastasios Tefas. Autoencoder-driven spiral representation learning for gravitational wave surrogate modelling. *Neurocomputing*, 491:67–77, June 2022.
- [25] Stefano Schmidt, Matteo Breschi, Rossella Gamba, Giulia Pagano, Piero Rettegno, Gunnar Riemenschneider, Sebastiano Bernuzzi, Alessandro Nagar, and Walter Del Pozzo. Machine learning gravitational waves from binary black hole mergers. *Phys. Rev. D*, 103:043020, Feb 2021.
- [26] Raimon Luna, Miquel Llorens-Monteagudo, Ana Lorenzo-Medina, Juan Calderón Bustillo, Nicolas Sanchis-Gual, Alejandro Torres-Forné, José A. Font, Carlos A. R. Herdeiro, and Eugen Radu. Numerical relativity surrogate waveform models for exotic compact objects: The case of head-on mergers of equal-mass proca stars. *Phys. Rev. D*, 110:024004, Jul 2024.
- [27] Joan Fontbuté, Tomas Andrade, Raimon Luna, Juan Calderón Bustillo, Gonzalo Morras, Santiago Jaraba, Juan García-Bellido, and Germán López Izquierdo. A numerical-relativity surrogate model for hyperbolic encounters of black holes: challenges in parameter estimation, 2024.
- [28] Tim Grimbergen, Stefano Schmidt, Chinmay Kalaghatgi, and Chris van den Broeck. Generating higher order modes from binary black hole mergers with machine learning, 2024.
- [29] Scott E. Field, Chad R. Galley, Jan S. Hesthaven, Jason Kaye, and Manuel Tiglio. Fast prediction and evaluation of gravitational waveforms using surrogate models. *Phys. Rev. X*, 4:031006, Jul 2014.
- [30] Vijay Varma, Scott E. Field, Mark A. Scheel, Jonathan Blackman, Davide Gerosa, Leo C. Stein, Lawrence E. Kidder, and Harald P. Pfeiffer. Surrogate models for precessing binary black hole simulations with unequal masses. *Phys. Rev. Res.*, 1:033015, Oct 2019.
- [31] Michael Boyle and Mark Scheel. The sxs package, June 2024.
- [32] Patricia Schmidt, Frank Ohme, and Mark Hannam. Towards models of gravitational waveforms from generic binaries: II. modelling precession effects with a single effective precession parameter. *Physical Review D*, 91(2), January 2015.
- [33] Bernhard Burgstaller and Friedrich Pillichshammer. The average distance between two points. *Bulletin of the Australian Mathematical Society*, 80(3):353–359, 2009.
- [34] Naomi Altman and Martin Krzywinski. The curse(s) of dimensionality. *Nature Methods*, 15(6):399–400, Jun 2018.
- [35] Rui Silva, Osvaldo Gramaxo Freitas, and Pedro Melo-Pinto. Boosting the performance of SOTA convolution-based networks with dimensionality reduction: An application on hyperspectral images of wine grape berries. *Intelligent Systems with Applications*, 19:200252, 2023.
- [36] V. Argyriou R. Dupre and D. Greenhill. Prediction of physics simulation using dimensionality reduction and regression. *Journal of Graphics Tools*, 17(3):99–110, 2013.
- [37] Ariana Mendible, Steven L. Brunton, Aleksandr Y. Aravkin, Wes Lowrie, and J. Nathan Kutz. Dimensionality reduction and reduced-order modeling for traveling wave physics. *Theoretical and Computational Fluid Dynamics*, 34(4):385–400, 2020.
- [38] Dor Bank, Noam Koenigstein, and Raja Giryes. Autoencoders, 2021.
- [39] Leland McInnes, John Healy, and James Melville. Umap: Uniform manifold approximation and projection for dimension reduction, 2020.
- [40] Svante Wold, Kim Esbensen, and Paul Geladi. Principal component analysis. *Chemometrics and Intelligent Laboratory Systems*, 2(1):37–52, 1987. Proceedings of the Multivariate Statistical Workshop for Geologists and Geochemists.
- [41] Ferath Kherif and Adeliya Latypova. Chapter 12 - principal component analysis. In Andrea Mechelli and Sandra Vieira, editors, *Machine Learning*, pages 209–225. Academic Press, 2020.
- [42] Takuya Akiba, Shotaro Sano, Toshihiko Yanase, Takeru Ohta, and Masanori Koyama. Optuna: A next-generation hyperparameter optimization framework. In *Proceedings of the 25th ACM SIGKDD International*

Conference on Knowledge Discovery and Data Mining, 2019.

- [43] Hong Liu, Zhiyuan Li, David Hall, Percy Liang, and Tengyu Ma. Sophia: A scalable stochastic second-order optimizer for language model pre-training, 2024.
- [44] Leslie N. Smith. Cyclical learning rates for training neu-

ral networks, 2017.

- [45] Pavel Izmailov, Dmitrii Podoprikin, Timur Garipov, Dmitry Vetrov, and Andrew Gordon Wilson. Averaging weights leads to wider optima and better generalization, 2019.